



Experimental Study of a Joukowsky Airfoil

AUTHORS

Mohammad Zandsalimy

December 9, 2021

Abstract

The flow characteristics over a two dimensional model of a Joukowski airfoil are studied experimentally in a low speed wind tunnel. This experiment is conducted to measure the pressure coefficients in different chord-wise locations on the upper and lower surfaces of the airfoil. Experiments were carried out by varying the angle of attack, from -6 to 16 degrees. The pressure distribution on the upper surface changes significantly at higher angles of attack (due to stall). The upper surface suction causes an adverse pressure gradient especially for higher angles of attack, resulting in rapid decay of kinetic energy over the upper surface, leading to a thicker wake and higher turbulence level. The test covered a range of Reynolds number from 300,000 to 600,000. Further, the lift and drag forces are measured using an external balance. The tests are conducted in a closed loop wind tunnel with no flow visualization possibility. The external load cell was calibrated to reduce the systematic errors in the measurement of lift and drag.



Contents

Abstract	i
List of Figures	iii
List of Tables	iv
Nomenclature	v
1 Introduction	1
1.1 Objectives	1
1.2 Facility Description	2
1.3 Airfoil Characteristics	3
2 Theory	5
3 Approach	6
3.1 Liquid Properties	9
3.2 Wind Speed and Reynolds Calculation	9
3.3 Lift and Drag Calculation	10
4 Results	11
5 Discussion	14
5.1 A. Drag and Lift Coefficients vs. Angle of Attack	15
5.2 B. Pressure Coefficients vs. x	17
5.3 C. Integrate Pressure Coefficients	19
5.4 D. Drag Coefficient vs. Re	21
5.5 E. Uncertainty Analysis	22
5.5.1 Zero order uncertainty	23
5.5.2 First order uncertainty	23
5.5.3 Nth order uncertainty	24
6 Conclusion	25
References	26



List of Figures

1	Typical airfoil characteristics.	1
2	Data acquisition, fan controller, and Betz manometer.	2
3	Close up of the Betz manometer.	3
4	External load cell.	3
5	Wind tunnel test section with the airfoil inside.	4
6	Multi-tube manometer filled with Ethyl Alcohol.	5
7	Drag calibration data.	7
8	Lift calibration data.	8
9	$\alpha = -6.0^\circ$	12
10	$\alpha = -4.0^\circ$	12
11	$\alpha = -2.0^\circ$	12
12	$\alpha = 0.0^\circ$	12
13	$\alpha = 2.0^\circ$	12
14	$\alpha = 4.0^\circ$	12
15	$\alpha = 6.0^\circ$	13
16	$\alpha = 8.0^\circ$	13
17	$\alpha = 10.0^\circ$	13
18	$\alpha = 12.0^\circ$	13
19	$\alpha = 14.0^\circ$	13
20	$\alpha = 16.0^\circ$	13
21	Lift coefficient vs. angle of attack.	16
22	Drag coefficient vs. angle of attack.	16
23	Drag polar.	17
24	C_p vs. tap location at $\alpha = 12.0^\circ$.	18
25	C_p vs. tap location at $\alpha = 6.0^\circ$.	19
26	C_d vs. Reynolds number.	22

List of Tables

1	Typical airfoil characteristics.	4
2	Drag calibration data.	6
3	Lift calibration data.	8
4	Liquid properties at $20^{\circ}C$	9
5	Lift and drag force vs. angle of attack.	11
6	Multi-tube manometer reading at $\alpha = 12.0^{\circ}$.	14
7	Drag and Lift vs. q at $\alpha = -4.0^{\circ}$ (minimum drag).	14
8	Calibrated lift and drag forces per unit span vs. angle of attack.	15
9	Pressure and C_p vs. tap number at $\alpha = 12.0^{\circ}$.	18
10	Pressure and C_p vs. tap number at $\alpha = 6.0^{\circ}$.	19
11	Data used for C_l calculation from C_p at $\alpha = 12.0^{\circ}$.	20
12	Data used for C_l calculation from C_p at $\alpha = 6.0^{\circ}$.	21
13	Drag coefficient vs. Reynolds number.	21



Nomenclature

α	Angle of Attack
μ	Dynamic Viscosity
ν	Kinematic Viscosity
ρ	Density
θ	Angle of an Arbitrary Panel with Chord
C_a	Axial Force Coefficient
C_d	Drag Coefficient per Unit Span
C_f	Surface Friction Factor
C_l	Lift Coefficient per Unit Span
C_n	Normal Force Coefficient
C_p	Pressure Coefficient
D	Drag Force
g	Gravity Acceleration
h	Liquid Column Height
L	Lift Force
P	Pressure
q	Betz Manometer Water Column Height in mm
Re	Reynolds Number
S	Length of an Arbitrary Panel
s	Wing Span
V_t	Test Section Inlet Average Velocity
C	chord
StDev	Standard Deviation



1 Introduction

Study of the fluid flow over curved boundaries is important in various industrial applications including turbo-machinery, aircraft, boats, heat exchangers, and many more. Airfoils are examples of objects with curved boundaries used in aircraft to produce lift. Different characteristics of airfoils are presented in Fig. 1. There are three different methods of analyzing fluid flow over objects; analytical approaches, numerical, and experimental methods. Because the analytical procedures are limited in the determination of some parameters such as maximum lift coefficient, characteristics after stall, determination of zero lift angle of attack, and pitching moment, numerical and experimental methods are utilized more often. Both of these methodologies have their own limitations. However, conducting experimental studies are essential and are required for data validation. Experiments on airfoils are conducted in wind tunnels to study the fluid flow over the airfoil and resulting aerodynamic forces. In the present lab, pressure distribution, lift, and drag forces on a Joukowski airfoil are measured and compared with existing theories and the results of flat plate. The experiments are carried out in a range of Reynolds numbers of 300,000 to 600,000 and the angle of attack of -6 to 16 degrees.

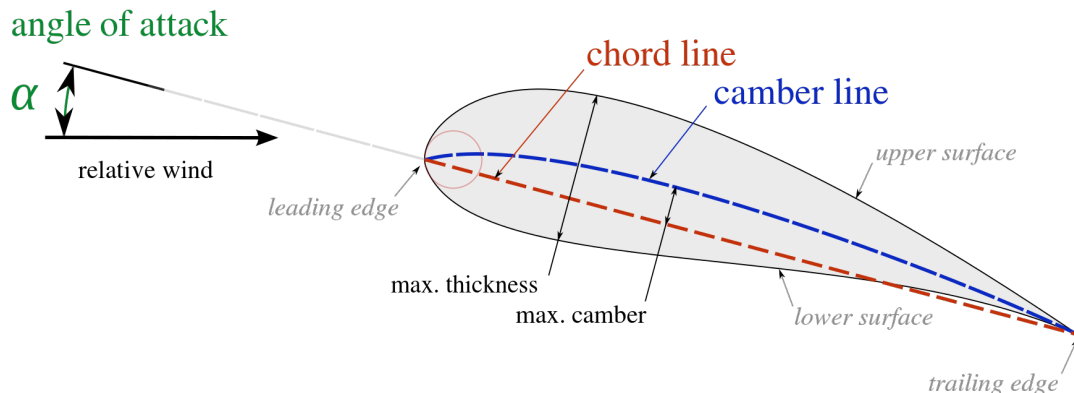


Figure 1: Typical airfoil characteristics.

1.1 Objectives

The main objectives of this experiment are:

- Conduct experiments on a 2D Joukowski airfoil
- Measure pressure distribution over the upper and lower surfaces
- Calculate lift and drag coefficients with pressure distribution
- Measure lift and drag forces using an external load cell

- Compare the results with available theories
- Study the stall phenomena
- Analysis of uncertainty
- Reduction of data and presentation

1.2 Facility Description

The test facility includes a closed loop low speed wind tunnel located at the University of British Columbia. There are various measurement tools available for this experiment. A photo of the data acquisition PC, fan rpm controller, as well as the Betz manometer is presented in Fig. 2. The wind tunnel has a rectangular test section. For such experimental studies utilizing wind tunnels, an important test before anything else is to measure the turbulence intensity in the wind tunnel test section. Unfortunately, this is not a part of the present study and we will trust that turbulence intensity is low enough. The Betz manometer measures the pressure difference between test section entrance and outside in millimeters of water. A photo of this manometer is presented in Fig. 3. The external balance used for lift and drag measurement is presented in Fig. 4. Also, in this figure the tubes connecting pressure taps to the manometer are seen.

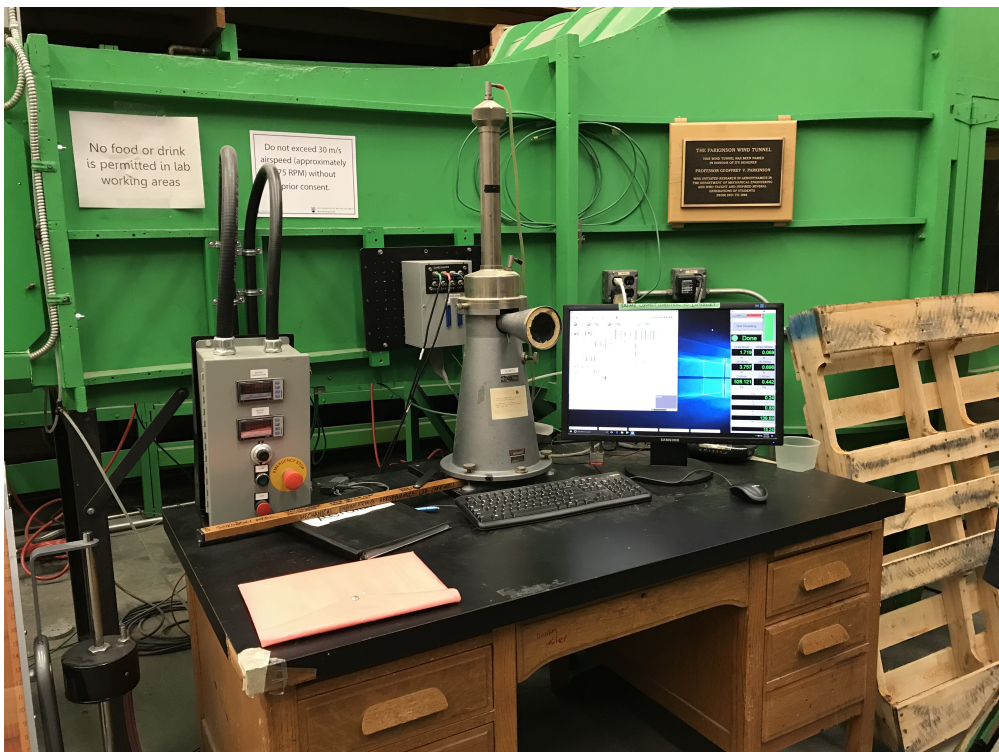


Figure 2: Data acquisition, fan controller, and Betz manometer.



Figure 3: Close up of the Betz manometer.

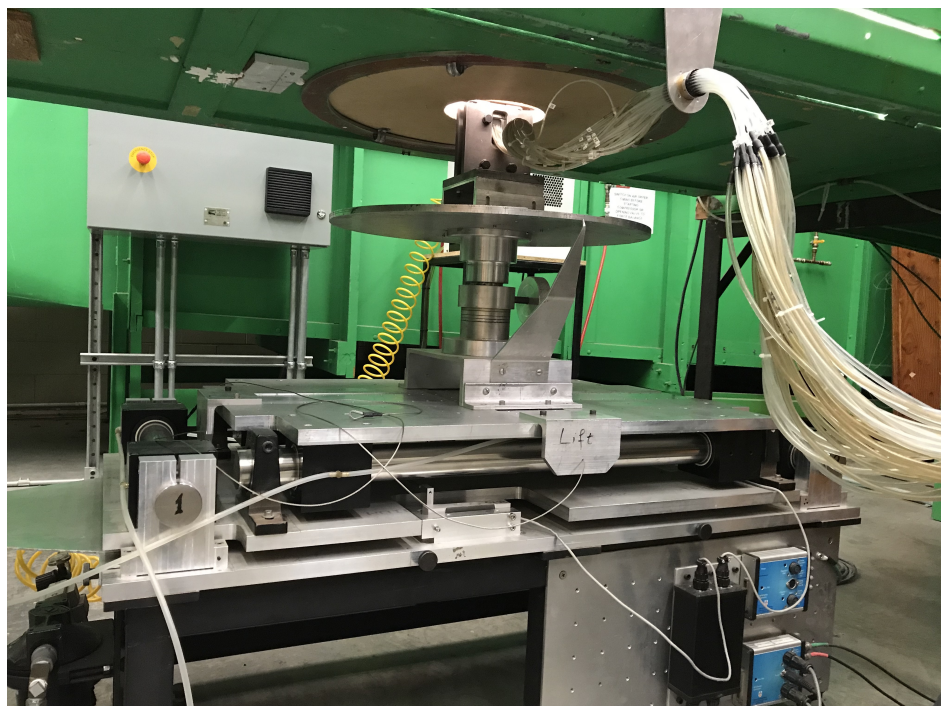


Figure 4: External load cell.

1.3 Airfoil Characteristics

Tests are carried out on a Joukowski airfoil with a chord of 0.3075 m. The airfoil has a span of 0.6858 m which is assumed to be high enough for a 2 dimensional flow at the middle of the span. The thickness of the airfoil is 11.1% of the chord and maximum camber is 2.4%

of the chord. There are 36 pressure taps with 24 taps on the suction surface and 12 on the pressure surface. The locations of pressure taps are indicated in Table 1. A photograph of the airfoil inside the wind tunnel test section is presented in Fig. 5. The pressure taps are connected to a multi-tube manometer filled with Ethyl Alcohol. This manometer is tilted exactly 30 degrees with the vertical plane for a more sensitive pressure reading. As a result of this, the change in height of liquid in each tube will be more and thus a more accurate reading. A photo of the multi-tube manometer is presented in Fig. 6.

Table 1: Typical airfoil characteristics.

Suction Surface		Pressure Surface	
Tap no.	x/C %	Tap no.	x/C %
1	0.0	13	38.5
2	0.4	14	43.4
3	1.6	15	48.4
4	3.3	16	53.4
5	5.0	17	58.4
6	7.1	18	63.4
7	9.9	19	68.4
8	13.5	20	73.4
9	18.5	21	78.4
10	23.5	22	83.3
11	28.5	23	88.3
12	33.5	24	93.3



Figure 5: Wind tunnel test section with the airfoil inside.



Figure 6: Multi-tube manometer filled with Ethyl Alcohol.

2 Theory

The drag force is the component of force on a body acting parallel to the direction of free stream. The drag coefficient C_d is the ratio of drag force to the wetted area of a wing times the dynamic head of free stream flow. If compressibility and free surface effects are neglected, drag coefficient is a function of Reynolds number only. The total drag force is the sum of the friction drag and pressure drag. Lift force acts on an immersed body normal to the relative free stream. The lift coefficient C_l is the ratio of lift force to the wetted area of a wing times the dynamic head of free stream flow. The lift coefficient may be calculated from the pressure distributions on the upper and lower surfaces as well. Pitching moment is the moment acting in the plane containing the lift and the drag. It is positive when it tends to increase the angle of attack. Coefficient of pitching moment is the ratio of Pitching moment to wetted area times free stream dynamic head times chord.

3 Approach

The first step for a successful experimental testing is to calibrate the measurement tool to reduce the systematic errors as much as possible. The static calibration is carried out for the external balance. This balance should be calibrated in two directions; parallel to test section flow (drag calibration) and normal to the flow (lift calibration). A range of loads are applied to get the relation between loads and the reading of the data acquisition system. The weights applied to the balance for drag calibration and the data readings are presented in table 2. Note that the measured values of the data acquisition system have units of Newtons, however, for the sake of this lab we will assume that we don't know the units. The standard deviation of measurement is also presented in this table. By plotting the data in Fig. 7 we can estimate any value of reading vs. the actual force with a simple linear relation fit. This relation is found to be as Eq. 1 using Matlab software. In this equation, $D(x)$ is the actual drag force and x is the reading value. Also, the uncertainty is the maximum value of the standard deviation.

Table 2: Drag calibration data.

Mass [kg]	Weight [N]	Measured Value	Drag StDev
0.113	1.109	1.159	0.022
0.313	3.071	3.094	0.017
0.513	5.033	5.053	0.019
0.713	6.995	6.995	0.017d
0.913	8.957	8.955	0.02
1.113	10.919	10.922	0.02
1.513	14.843	14.844	0.015
1.913	18.767	18.779	0.019
2.113	20.729	20.713	0.019
2.613	25.634	25.614	0.021
3.113	30.539	30.519	0.021
3.513	34.463	34.426	0.02
3.913	38.387	38.35	0.022

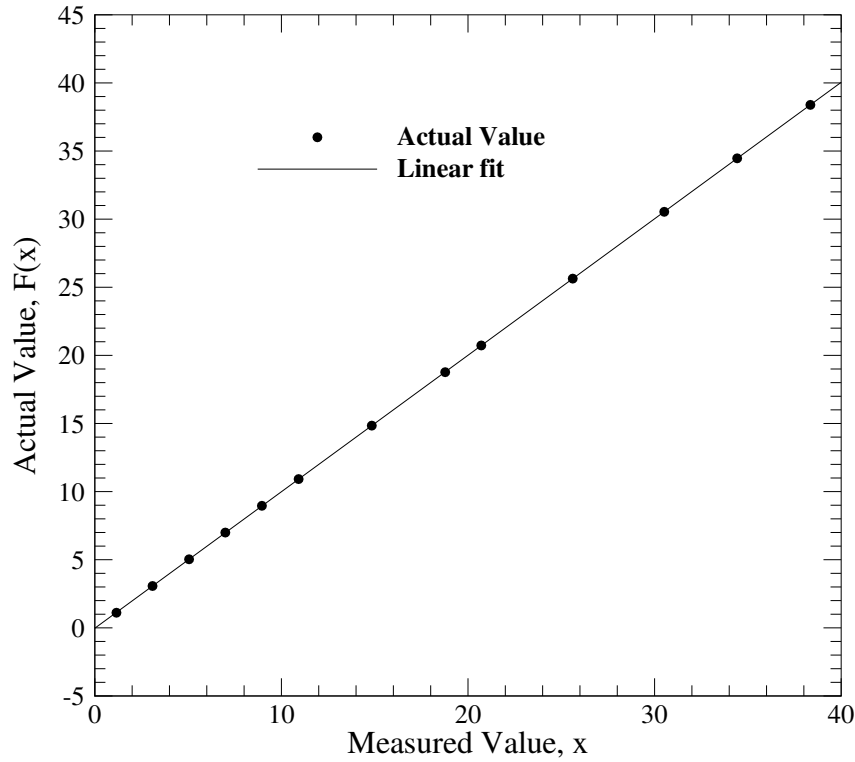


Figure 7: Drag calibration data.

$$D(x) = 1.001792x - 0.028477 \pm 0.022 \quad N \quad (1)$$

The same procedure is repeated for the lift calibration. The weights applied to the balance for lift calibration and the data readings are presented in table 3. The standard deviation of measurement is also presented in this table. By plotting the data in Fig. 8 we can estimate any value of reading vs. the actual force with a simple linear relation fit. This relation is found to be as Eq. 2 using Matlab software. In this equation, $L(x)$ is the actual lift force and x is the reading value. Also, the uncertainty is the maximum value of the standard deviation.

Table 3: Lift calibration data.

Mass [kg]	Weight [N]	Measured Value	Lift StDev
0.113	1.109	1.143	0.023
0.313	3.071	3.076	0.018
0.513	5.033	4.986	0.028
0.713	6.995	6.929	0.031
0.913	8.957	8.896	0.03
1.113	10.919	10.845	0.027
1.513	14.843	14.759	0.02
1.913	18.767	18.702	0.027
2.113	20.729	20.685	0.022
2.613	25.634	25.545	0.021
3.113	30.539	30.51	0.022
3.513	34.463	34.473	0.024
3.913	38.387	38.369	0.032

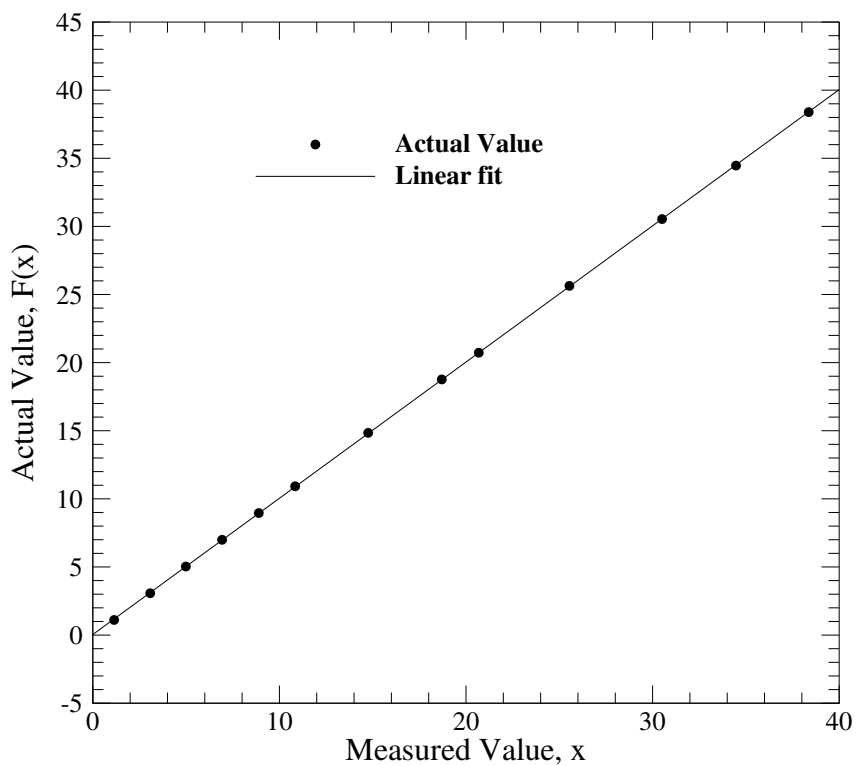


Figure 8: Lift calibration data.

$$L(x) = 1.000000x + 0.040975 \pm 0.032 \quad N \quad (2)$$

3.1 Liquid Properties

The temperature of testing area was recorded to be $20^{\circ}C$. Using standard liquid property tables we can construct a useful table for the calculations of pressure and velocity. The properties of air, water, and ethyl alcohol at $20^{\circ}C$ are presented in table 4.

Table 4: Liquid properties at $20^{\circ}C$.

Liquid	Density (ρ) kg/m^3	Dynamic Ciscosity (μ) kg/ms	Kinematic Viscosity (ν) m^2/s
Air	1.2047	1.8205×10^{-5}	1.5111×10^{-5}
Water	998.21	1.0020×10^{-3}	1.0030×10^{-6}
Ethanol	789.20	1.1440×10^{-3}	1.5000×10^{-6}

3.2 Wind Speed and Reynolds Calculation

The Betz manometer measures a pressure difference between the entrance of test section and outside of the wind tunnel in millimeters of water (q). Using this measurement we can calculate the average wind speed inside the test section as well as the Reynolds number. Let's write a Bernoulli relation between outside of the wind tunnel (o) and the test section (t) as in Eq. 3.

$$P_o + \frac{1}{2}\rho_{air}V_o^2 = P_t + \frac{1}{2}\rho_{air}V_t^2 \quad (3)$$

in which V_o is zero. As a result, we can write;

$$P_o - P_t = \frac{1}{2}\rho_{air}V_t^2 \quad (4)$$

and then

$$V_t = \sqrt{\frac{P_o - P_t}{\frac{1}{2}\rho_{air}}} \quad (5)$$

The static pressure difference of a column of water can be expressed as;

$$\Delta P = \rho_{water}gh \quad (6)$$

in which g is the gravitational acceleration and h is the height of the water column. Combining equations 5 and 6;

$$V_t = \sqrt{2gh \frac{\rho_{water}}{\rho_{air}}} \quad (7)$$



Let's use $g = 9.81 \text{ m/s}^2$, and simplify this equation to get;

$$V_t = 4.032\sqrt{h} \quad (8)$$

in which h is in millimeters of water change the unit of h to meters.

Now that the average wind speed inside the test section is known, we can calculate the Reynolds number as follows;

$$Re = \frac{V_t C}{\nu_{air}} \rightarrow Re = 82048.930\sqrt{h} \quad (9)$$

3.3 Lift and Drag Calculation

There are two possible methods for calculating lift and drag coefficients in the present study; using the external load cell and using static pressure taps. The external balance measures the resulting drag and lift forces, which we can use to calculate C_l and C_d using the definitions of lift and drag coefficients as follows;

$$C_l = \frac{L}{\frac{1}{2}\rho_{air}V_t^2 C} \quad (10)$$

$$C_d = \frac{D}{\frac{1}{2}\rho_{air}V_t^2 C} \quad (11)$$

Also, the pressure coefficient is defined as the following equation;

$$C_p = \frac{P - P_o}{\frac{1}{2}\rho_{air}V_t^2} \quad (12)$$

Using pressure coefficients is another method to calculate lift and drag coefficients. In this method, we need to find normal (C_n) and axial (C_a) force coefficients. Then, pressure coefficients can be integrated over the airfoil utilizing airfoil panels.

$$C_n = \frac{1}{C} \left[\int_0^C (C_{p,l} - C_{p,u}) dx + \int_0^C \left(C_{f,u} \frac{dy_u}{dx} - C_{f,l} \frac{dy_l}{dx} \right) dx \right] \quad (13)$$

$$C_a = \frac{1}{C} \left[\int_0^C \left(C_{p,u} \frac{dy_u}{dx} - C_{p,l} \frac{dy_l}{dx} \right) dx + \int_0^C (C_{f,l} + C_{f,u}) dx \right] \quad (14)$$

in which l and u subscripts denote lower and upper surfaces of the airfoil. For the purpose of this experiment we can neglect the effects of surface friction factor (C_f). As a result;

$$C_n = \frac{1}{C} \int_0^C (C_{p,l} - C_{p,u}) dx \quad (15)$$

$$C_a = \frac{1}{C} \int_0^C \left(C_{p,u} \frac{dy_u}{dx} - C_{p,l} \frac{dy_l}{dx} \right) dx \quad (16)$$

Now we can calculate lift and drag coefficients;

$$C_l = C_n \cos \alpha - C_a \sin \alpha \quad (17)$$

$$C_d = C_n \sin \alpha + C_a \cos \alpha \quad (18)$$

We have to devise a method for integrating discrete pressure coefficients over the airfoil. For this purpose, we need to divide the airfoil surface into a number of panels. Then, using the length and angle of each panel (Eqs. 19 and 20) we can calculate C_p as in Eq. 21.

$$S = \sqrt{(y_2 - y_1)^2 + (x_2 - x_1)^2} \quad (19)$$

$$\theta = \tan \left(\frac{y_2 - y_1}{x_2 - x_1} \right) \quad (20)$$

$$\begin{cases} C_n = \sum C_{p_i} \cos(\theta_i) \frac{S_i}{C} \\ C_a = \sum C_{p_i} \sin(\theta_i) \frac{S_i}{C} \end{cases} \quad (21)$$

4 Results

In this section, the results of the experiments are presented. With the Betz manometer kept at $q = 30$ millimeters of water ($Re = 4.5 \times 10^5$), the lift and drag forces are measured in a range of α of -6 to 16 degrees. The results of this measurement is presented in table 5. The multi-tube manometer pressure readings are presented in Figs. 9 to 20.

Table 5: Lift and drag force vs. angle of attack.

Angle of Attack [°]	Drag Reading	Drag StDev	Lift Reading	Lift StDev
-6	1.289	0.055	-8.498	0.426
-4	1.091	0.057	1.730	0.557
-2	1.150	0.031	12.784	0.381
0	1.461	0.031	23.954	0.414
2	1.937	0.041	34.467	0.348
4	2.697	0.080	44.540	0.479
6	3.692	0.120	53.714	0.512
8	4.915	0.145	62.714	0.711
10	6.151	0.161	70.458	0.706
12	7.579	0.277	74.438	0.810
14	14.527	9.094	63.857	10.342
16	18.082	6.063	62.438	6.224



Figure 9: $\alpha = -6.0^\circ$ Figure 10: $\alpha = -4.0^\circ$ Figure 11: $\alpha = -2.0^\circ$ Figure 12: $\alpha = 0.0^\circ$ Figure 13: $\alpha = 2.0^\circ$ Figure 14: $\alpha = 4.0^\circ$

Figure 15: $\alpha = 6.0^\circ$ Figure 16: $\alpha = 8.0^\circ$ Figure 17: $\alpha = 10.0^\circ$ Figure 18: $\alpha = 12.0^\circ$ Figure 19: $\alpha = 14.0^\circ$ Figure 20: $\alpha = 16.0^\circ$

Keeping $q = 30$ millimeters of water and setting the angle of attack to 12.0° , we recorded the static pressures through the multi-tube manometer. These results are presented in table 6. Further, a conversion to millimeters has been conducted for convenience. The reference pressure is 9.2 inch equal to 233.68 mm.

Table 6: Multi-tube manometer reading at $\alpha = 12.0^\circ$.

Tap No.	h [inch]	h [mm]	Tap No.	h [inch]	h [mm]
1	15.65	397.51	19	8.99	228.35
2	17.60	447.04	20	8.89	225.81
3	15.61	396.49	21	8.82	224.03
4	14.51	368.55	22	8.76	222.50
5	12.95	328.93	23	8.72	221.49
6	12.35	313.69	24	8.70	220.98
7	11.81	299.97	25	6.82	173.23
8	11.31	287.27	26	6.82	173.23
9	10.90	276.86	27	7.19	182.63
10	10.60	269.24	28	7.41	188.21
11	10.35	262.89	29	7.68	195.07
12	10.12	257.05	30	7.80	198.12
13	9.90	251.46	31	7.88	200.15
14	9.70	246.38	32	7.91	200.91
15	9.52	241.81	33	7.96	202.18
16	9.46	240.28	34	8.00	203.20
17	9.21	233.93	35	8.03	203.96
18	9.10	231.14	36	8.05	204.47

With the airfoil angle of attack at 4.0° (minimum drag), lift and drag forces are measured at different values of q . These results are presented in table 7.

Table 7: Drag and Lift vs. q at $\alpha = -4.0^\circ$ (minimum drag).

q	Lift Reading	Lift StDev	Drag Reading	Drag StDev
25.0	1.552	0.387	0.933	0.041
29.0	1.814	0.459	1.053	0.041
38.0	2.495	0.653	1.365	0.054
34.0	2.151	0.718	1.229	0.048
43.0	2.852	0.663	1.531	0.055
47.1	2.988	0.773	1.671	0.070
53.1	3.527	0.789	1.880	0.076

5 Discussion

In the current section the forces are calibrated and used to answer the questions.

5.1 A. Drag and Lift Coefficients vs. Angle of Attack

We can calibrate the data in table 5 using Eqs. 1 and 2. Then, using Eqs. 10 and 11, the lift and drag coefficients are calculated. Keep in mind that we have to calculate the lift and drag coefficients per unit span (s). This means that we need to divide the calibrated lift and drag by the span of the airfoil ($s = 0.6858 \text{ m}$). The theoretical lift coefficient of a general Joukowski airfoil is presented as Eq. 22. These results are presented in table 8 and plotted in Figs. 21 and 22. Also, Fig. 21 shows the theoretical value of C_l which correlates well with our experiment. Furthermore, Fig. 23 shows the plot of C_l vs. C_d which is known as drag polar. The wind speed for this test is 22.08 m/s . As seen in Fig. 21 the maximum lift occurs at $\alpha = 12.0$ which means after this angle, stall happens. This is also obvious by looking at the standard deviations in lift and drag calculations. At angles of attack higher than 12.0° , standard deviation has a sudden jump which means that the apparatus has undergone serious oscillations. Also, the multi-tube manometer shows a constant pressure for the upper surface of the airfoil at $\alpha = 14.0, 16.0$. This means that flow separation occurs from the leading edge of the airfoil.

$$C_l = 2\pi \left(1 + 0.77 \frac{\text{thickness}}{\text{chord}} \right) \left(\alpha + 2.0 \frac{\text{camber}}{\text{chord}} \right) \quad (22)$$

Table 8: Calibrated lift and drag forces per unit span vs. angle of attack.

Angle of Attack [°]	Drag [N]	Lift [N]	C_d	C_l
-6	1.263	-8.466	0.02039	-0.13665
-4	1.064	1.7620	0.01717	0.02844
-2	1.124	12.816	0.01814	0.20687
0	1.435	23.986	0.02316	0.38717
2	1.912	34.499	0.03086	0.55687
4	2.673	44.572	0.04315	0.71946
6	3.670	53.746	0.05924	0.86755
8	4.895	62.746	0.07901	1.01282
10	6.134	70.490	0.09901	1.13782
12	7.564	74.470	0.12209	1.20206
14	14.525	63.889	0.23446	1.03127
16	18.086	62.470	0.29194	1.00836

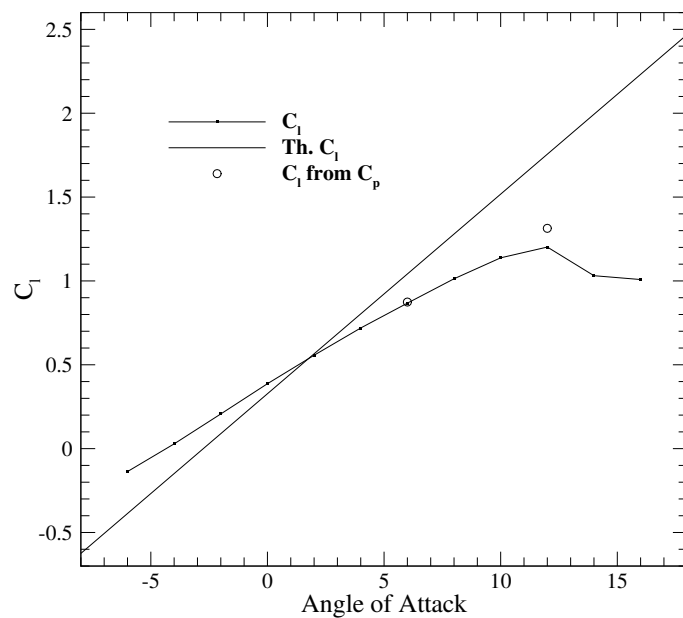


Figure 21: Lift coefficient vs. angle of attack.

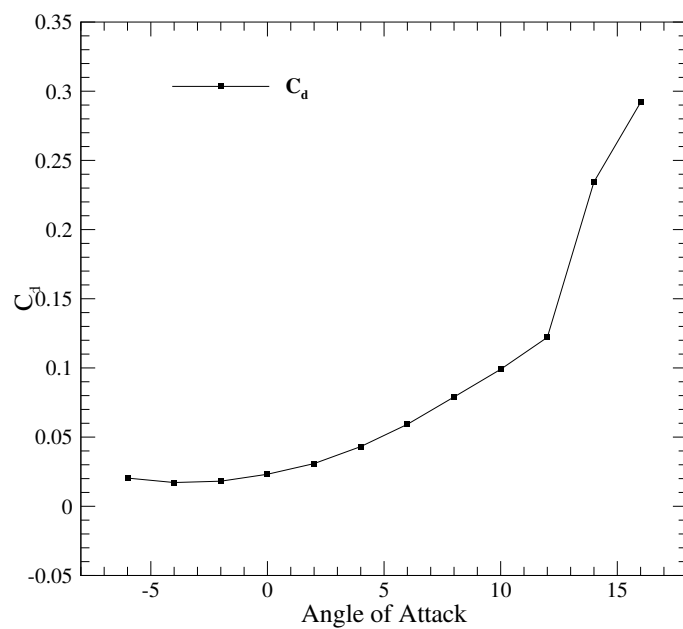


Figure 22: Drag coefficient vs. angle of attack.

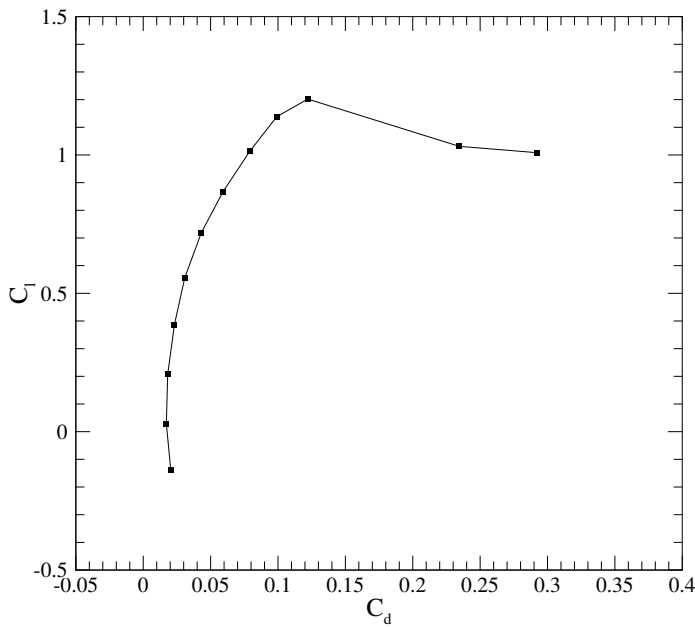


Figure 23: Drag polar.

5.2 B. Pressure Coefficients vs. x

At $\alpha = 12.0^\circ$, tap pressures were recorded using the multi-tube manometer. The manometer is tilted 30 degrees with the normal plane. The pressure difference between a tube and the reference pressure can be calculated using the following procedure.

$$\begin{aligned}\Delta P &= \rho_{eth}g \cos(30^\circ)(h_{ref} - h) \\ \Delta P &= 170.304(h_{ref} - h)\end{aligned}\quad (23)$$

in which h is in inches. Further, using Eq. 12 we can calculate pressure coefficients for each of the pressure taps. These results are presented in table 9. The pressure coefficients are plotted vs. tap location relative to the airfoil chord in Fig. 24. The same experiment was repeated for $\alpha = 6.0^\circ$ and the results are presented in table 10 and Fig. 25.

Table 9: Pressure and C_p vs. tap number at $\alpha = 12.0^\circ$.

Tap No.	Pressure [Pa]	C_p	Tap No.	Pressure [Pa]	C_p	Tap No.	Pressure [Pa]	C_p
1	-1098.459	-3.739	13	-119.213	-0.406	25	405.323	1.380
2	-1430.552	-4.870	14	-85.152	-0.290	26	405.323	1.380
3	-1091.647	-3.716	15	-54.497	-0.186	27	342.311	1.165
4	-904.313	-3.078	16	-44.279	-0.151	28	304.844	1.038
5	-638.639	-2.174	17	-1.703	-0.006	29	258.862	0.881
6	-536.457	-1.826	18	17.030	0.058	30	238.425	0.812
7	-444.493	-1.513	19	35.764	0.122	31	224.801	0.765
8	-359.341	-1.223	20	52.794	0.180	32	219.692	0.748
9	-289.516	-0.986	21	64.715	0.220	33	211.177	0.719
10	-238.425	-0.812	22	74.934	0.255	34	204.365	0.696
11	-195.849	-0.667	23	81.746	0.278	35	199.255	0.678
12	-156.679	-0.533	24	85.152	0.290	36	195.849	0.667

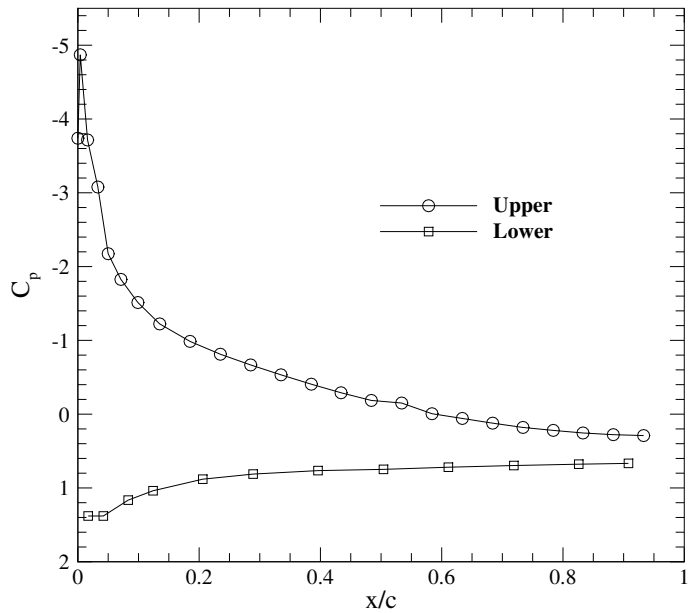
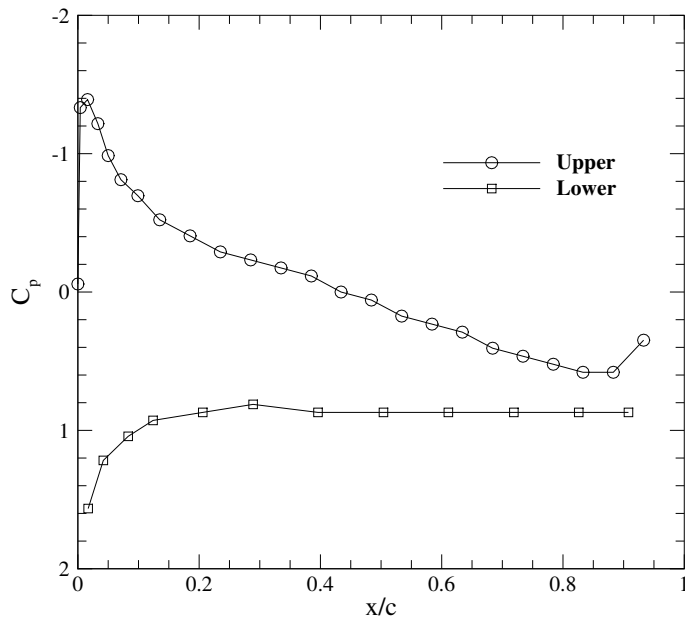
Figure 24: C_p vs. tap location at $\alpha = 12.0^\circ$.

Table 10: Pressure and C_p vs. tap number at $\alpha = 6.0^\circ$.

Tap No.	Pressure [Pa]	C_p	Tap No.	Pressure [Pa]	C_p	Tap No.	Pressure [Pa]	C_p
1	-17.030	-0.058	13	-34.061	-0.116	25	459.821	1.565
2	-391.699	-1.333	14	0.000	0.000	26	357.638	1.217
3	-408.730	-1.391	15	17.030	0.058	27	306.547	1.043
4	-357.638	-1.217	16	51.091	0.174	28	272.486	0.928
5	-289.517	-0.986	17	68.122	0.232	29	255.456	0.870
6	-238.426	-0.812	18	85.152	0.290	30	238.426	0.812
7	-204.365	-0.696	19	119.213	0.406	31	255.456	0.870
8	-153.274	-0.522	20	136.243	0.464	32	255.456	0.870
9	-119.213	-0.406	21	153.274	0.522	33	255.456	0.870
10	-85.152	-0.290	22	170.304	0.580	34	255.456	0.870
11	-68.122	-0.232	23	170.304	0.580	35	255.456	0.870
12	-51.091	-0.174	24	102.182	0.348	36	255.456	0.870

Figure 25: C_p vs. tap location at $\alpha = 6.0^\circ$.

5.3 C. Integrate Pressure Coefficients

Some relations are presented in Sec. 3.3 for the integration of C_p over an airfoil. However, for the present Joukowski airfoil, the y coordinates of the surface are not known. For the calculation of lift we can use a simpler version of such integration. According to Green's

flux theorem we can use the image of a curved section to calculate the pressure on a surface. As a result, just assume the airfoil as a flat plate and calculate C_l . With this assumption we will have $C_a = 0$. Also, we need to pay attention to the direction of the acting forces on each panel.

$$C_n = \sum C_{p_i} S_i \quad (24)$$

$$C_l = C_n \cos(\alpha) \quad (25)$$

The data is presented in table 11. The lift coefficient from this method is found to be $C_l = 1.3137$. The data for $\alpha = 6.0^\circ$ is presented in table 12. The lift coefficient from this method is found to be $C_l = 0.87406$. These points are shown in Fig. 21 with hollow circles. As seen in this figure, there is a good correlation between the results. The relative error between C_l in this section and the results of load cell is 9.3%.

Table 11: Data used for C_l calculation from C_p at $\alpha = 12.0^\circ$.

Tap No.	x/C	S	C_p	Tap No.	x/C	S	C_p
1	0.000	0.0040	-3.739	19	0.684	0.0500	0.122
2	0.004	0.0120	-4.870	20	0.734	0.0500	0.180
3	0.016	0.0170	-3.716	21	0.784	0.0490	0.220
4	0.033	0.0170	-3.078	22	0.833	0.0500	0.255
5	0.050	0.0210	-2.174	23	0.883	0.0500	0.278
6	0.071	0.0280	-1.826	24	0.933	0.0670	0.290
7	0.099	0.0360	-1.513	25	0.017	0.0295	1.380
8	0.135	0.0500	-1.223	26	0.042	0.0330	1.380
9	0.185	0.0500	-0.986	27	0.083	0.0410	1.165
10	0.235	0.0500	-0.812	28	0.124	0.0615	1.038
11	0.285	0.0500	-0.667	29	0.206	0.0825	0.881
12	0.335	0.0500	-0.533	30	0.289	0.0950	0.812
13	0.385	0.0490	-0.406	31	0.396	0.1075	0.765
14	0.434	0.0500	-0.290	32	0.504	0.1075	0.748
15	0.484	0.0500	-0.186	33	0.611	0.1075	0.719
16	0.534	0.0500	-0.151	34	0.719	0.1075	0.696
17	0.584	0.0500	-0.006	35	0.826	0.0945	0.678
18	0.634	0.0500	0.058	36	0.908	0.1330	0.667



Table 12: Data used for C_l calculation from C_p at $\alpha = 6.0^\circ$.

Tap No.	x/C	S	C_p	Tap No.	x/C	S	C_p
1	0	0.004	-0.058	19	0.684	0.05	0.406
2	0.004	0.012	-1.333	20	0.734	0.05	0.464
3	0.016	0.017	-1.391	21	0.784	0.049	0.522
4	0.033	0.017	-1.217	22	0.833	0.05	0.58
5	0.05	0.021	-0.986	23	0.883	0.05	0.58
6	0.071	0.028	-0.812	24	0.933	0.067	0.348
7	0.099	0.036	-0.696	25	0.017	0.0295	1.565
8	0.135	0.05	-0.522	26	0.042	0.033	1.217
9	0.185	0.05	-0.406	27	0.083	0.041	1.043
10	0.235	0.05	-0.29	28	0.124	0.0615	0.928
11	0.285	0.05	-0.232	29	0.206	0.0825	0.87
12	0.335	0.05	-0.174	30	0.289	0.095	0.812
13	0.385	0.049	-0.116	31	0.396	0.1075	0.87
14	0.434	0.05	0	32	0.504	0.1075	0.87
15	0.484	0.05	0.058	33	0.611	0.1075	0.87
16	0.534	0.05	0.174	34	0.719	0.1075	0.87
17	0.584	0.05	0.232	35	0.826	0.0945	0.87
18	0.634	0.05	0.29	36	0.908	0.133	0.87

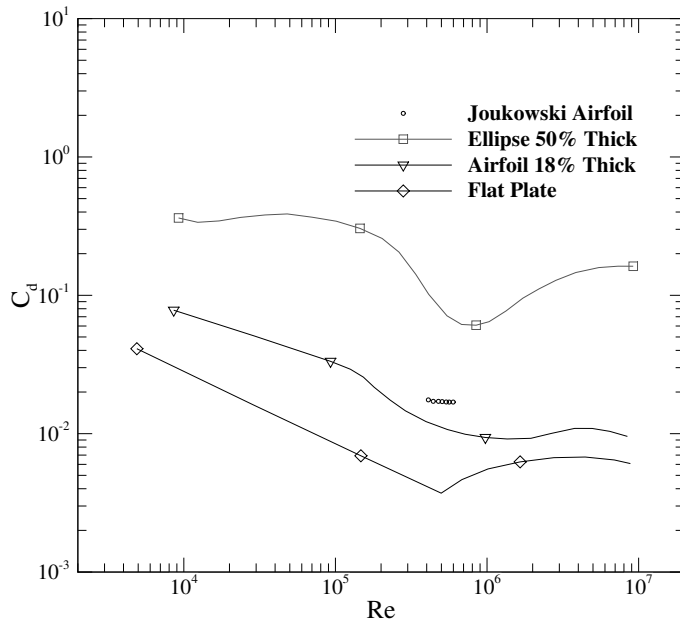
5.4 D. Drag Coefficient vs. Re

For this section, we have calculated C_d vs. Reynolds number. Do not forget that C_d should be reported per unit span. The results are presented in table 13. Fig. 26 shows a plot of C_d vs. Reynolds number. This plot also shows the drag coefficient of an arbitrary flat plate, an 18% thickness airfoil, and a 50% thickness ellipse. As seen in this figure, C_d from our experiment follows the same trend as the flat plate as well as the other airfoil. The flow is laminar before $Re = 5 \times 10^5$ and turbulent after that for the flat plate. Drag coefficient decreases with increasing Re for our airfoil which is similar to the other airfoil reported in this figure. If compressibility and free surface effects are neglected, drag coefficient is a function of Reynolds number only which is the case in our experiment.

Table 13: Drag coefficient vs. Reynolds number.

q [mm]	V_t [m/s]	Re	C_d
25.0	20.160	410245	0.01755
29.0	21.713	441847	0.01714
34.0	23.510	478423	0.01713
38.0	24.855	505784	0.01706
43.0	26.440	538031	0.01695
47.1	27.671	563097	0.01692
53.1	29.381	597888	0.01692



Figure 26: C_d vs. Reynolds number.

5.5 E. Uncertainty Analysis

The term uncertainty is used to refer to a “possible value that an error may have”. It is necessary to make a distinction between single sample and multiple sample uncertainty analysis. The distinction hinges on whether or not a “large” or “small” number of independent data points are taken at each test point and on how the data are handled. Uncertainties for the experimentally measured lift coefficient are evaluated in this section. The methodology for estimating uncertainties follows the AIAA S-071 Standard as presented in [1] for multiple tests (sections 6.1 and 6.3). Uncertainties include various parameters such as; reading errors, measurement errors, calibration error and so on. Sources of error of the present experiment can be summarized as:

- Measurement system errors
- Noise or random errors
- Reading errors
- Calibration errors
- Errors in airfoil geometry and manufacturing which accounts for the errors in pressure tap positions as well

Consider a variable x_i which has a known uncertainty δx_i . The form of representation of this variable and its uncertainty is:

$$x_i = \bar{x}_i \pm \delta x_i \quad [P\%] \quad (26)$$

In this equation, \bar{x}_i is the best estimate of x_i . Also, there is $P\%$ chance that this statement is true. Further, δx_i represents 2σ for a single sample analysis in which σ is the standard deviation of population of a possible data set.

The results R of the experiment is assumed to be calculated as a function of a number of independent parameters represented by:

$$R = R(x_1, x_2, \dots, x_m) \quad (27)$$

The effect of the uncertainty in a single measurement on the calculated results is:

$$\delta Rx_i = \frac{\partial R}{\partial x_i} \delta x_i \quad (28)$$

$\frac{\partial R}{\partial x_i}$ is the sensitivity coefficient for the results R with respect to measurement x_i . When several independent variables are used in the function of R, the individual terms are combined by RSS method.

$$\delta R = \left(\sum_{i=1}^m \left(\frac{\partial R}{\partial x_i} \delta x_i \right)^2 \right)^{0.5} \quad (29)$$

Unlike a multiple sample experiment, in which the variable error in a set of measurements can be determined from variance, simple sample experiments require an auxiliary experiment in order to estimate the variable component of the uncertainty. This usually takes the form of a set of independent observations of the process at a representative test condition over a representative interval of time. The principal difficulty here is finding σ , the standard deviation of the population from a smaller than infinite set of observations. σ is different from the standard deviation of the set of observations made in the auxiliary experiment, but can be estimated from it. In single sample uncertainty analysis, each measurement is assigned three uncertainty value; zero, first and Nth order uncertainties.

5.5.1 Zero order uncertainty

The zero order uncertainty of a measurement is the RSS combination of all the fixed and random uncertainty components introduced by the measuring system.

5.5.2 First order uncertainty

The first order uncertainty of a measurement describes the scatter that would be expected in a set of observation using the given apparatus and instrumentation system, while the observed process is running. The first order uncertainty includes all effects of process

unsteadiness as well as the variable error effects from the measuring system. The first order uncertainty interval must be measured in an auxiliary experiment.

5.5.3 Nth order uncertainty

The Nth order uncertainty of a result is a measure of its overall uncertainty, accounting for all sources of fixed and variable errors. This is the value that should be reported as the overall uncertainty. The Nth order uncertainty is calculated as the RSS combination of the first order uncertainty and the fixed errors from every source.

Now we can calculate the uncertainty in C_l from Sec. 5.1. For this purpose the uncertainties can be summarized as follows:

- Error in lift calibration, u_c .
- Error in reading the Betz manometer, $u_{Betz} = \frac{0.1}{2} = 0.05$. This manometer has a precision of 0.1 and the error is half of this precision.
- Error in the data acquisition system, u_{data} . This uncertainty is equal to the maximum value of standard deviation in the readings for lift, which is 0.032.
- Error in calculating V_t , u_{V_t} which is calculated from the following equation. Be sure to change the units of h to meters.

$$u_{V_t} = h \frac{\partial}{\partial h} (4.032\sqrt{h}) = 4.032 \frac{\sqrt{h}}{2} = 4.032 \frac{\sqrt{0.03}}{2} = 0.3492$$

The final uncertainty can be estimated using RSS method as follows;

$$\sigma = \sqrt{\left(\frac{\partial C_l}{\partial L} u_L\right)^2 + \left(\frac{\partial C_l}{\partial V_t} u_{V_t}\right)^2}$$

$$\sigma = \sqrt{\left(\frac{2}{\rho V_t^2 C} u_L\right)^2 + \left(\frac{-4L}{\rho V_t^3 C} u_{V_t}\right)^2}$$

For $\alpha = 12$ we can calculate the error as follows. This angle of attack has the maximum lift force which accounts for the highest error possible.

$$\sigma = \sqrt{\left(\frac{2}{1.2047 \times 22.08^2 \times 0.3075} 0.05\right)^2 + \left(\frac{-4 \times 74.470}{1.2047 \times 22.08^3 \times 0.3075} 0.3492\right)^2} = 0.0747 \quad (30)$$

As a result, the lift coefficient can be expressed as the following equation;

$$C_l = \bar{C}_l \pm 0.0747 \quad (31)$$



6 Conclusion

In the present experiment pressure, lift, and drag was measured over a Joukowski airfoil. The results of lift coefficient were different than theory which is due to the fact that theory falls short of including viscous effects as well as stall phenomena. Also, the lift coefficient calculated from pressure coefficients had about 10% difference with the lift coefficient from the external load balance. The airfoil experienced stall phenomenon at angles of attack greater than 12.0 degrees. This angle is typical in thin airfoils. Also, as seen in the multi-tube manometer for $\alpha = 14.0, 16.0$ degrees the upper surface of the airfoil has almost constant pressure. This means that the flow detaches from the leading edge of the airfoil, which again is a characteristic of thin airfoils. After stall, there is a sudden reduction in C_l . The values of drag coefficient were plotted against Reynolds number. The trend of the present experiment follows the trend of flat plates and a similar symmetric airfoil. C_d reduces as Re increases, which is a function of Re only. The uncertainty analysis of lift coefficient shows a value of 0.44 for the error of our experiments which is acceptable.

References

- [1] F. Stern, M. Muste, M.-L. Beninati, and W. E. Eichinger, “Summary of experimental uncertainty assessment methodology with example,” tech. rep., IIHR Report, 1999.